Generalized Analysis for a Class of Linear Interferometric Networks—Part I: Analysis

Otto Schwelb, *Senior Life Member, IEEE*

***Abstract*—A method is introduced to simplify the analysis and design of microwave and optoelectronic networks such as spectral filters, interferometric sensors, etc., comprised of 2 × 2 couplers, waveguides, reflectors, and mismatched interfaces. The key element which makes it possible to reduce topological complexity and rearrange a network into a chain of cascaded four-ports, is a generalized, single-mode lumped-element 2 × 2 coupler with arbitrary coupling paths. As a result, one can now enumerate and evaluate all possible feedback-assisted and resonant configurations. The emphasis is on providing a computationally efficient method of analysis applicable to a wide variety of networks, rather than on obtaining the simplest and most transparent analytical expressions for a particular configuration.**

***Index Terms*— Filter circuits, interferometric networks, network analysis, sensors.**

I. Introduction

MICROWAVE and optoelectronic circuits built with 2 × 2 couplers, reflectors, and transmission lines as building blocks are used in numerous applications such as spectral filters [1]–[4], interferometers [5]–[9], resonators [10]–[14], and recirculating delay lines [15], [16]. Ring resonators, both passive and active, comprised of 2 × 2 couplers terminated by reflecting elements and/or feedback lines, have received considerable attention in the literature [17]–[19]. Recently, a number of optical sensor configurations constructed from these building blocks have been analyzed analytically [20]–[23] and experimentally [24], [25]. The appropriate fabrication technology depends on operating wavelength, embedding, and size requirements. Existing realizations use metallic waveguides, microstrip, optical fibers, surface-wave technology, and bulk optics.

Scanning the literature, one sees a bewildering variety of interferometric circuits constructed from the above building blocks. In the past, these circuits have been analyzed either case by case or in groups that feature the same topology. In this paper, a generalized lumped-element 2 × 2 coupler is introduced, which permits one to "straighten out" the intricate and often intractable configurations into a cascaded set of four-ports, which are then treated by transmission matrix analysis. As an additional advantage, this regularization of the topology allows the enumeration and systematic evaluation of all possible feedback-assisted and resonant configurations that can be devised using the above building blocks.

The approach presented here favors computational efficiency to the detailed analysis of the individual circuit application. However, we shall demonstrate that analytic expressions for the scattering matrix elements can be obtained by simple inspection of a cascaded circuit. It will be assumed that the components operate in the linear regime and support a single mode, i.e., mode conversion or conversion between orthogonal polarizations is disregarded.

The network obtained by connecting the basic building blocks, called the cascaded network, is a four-port. Some of the ports of the cascaded network may be terminated or connected to each other through feedback lines. Accordingly, in addition to the cascaded network, we shall also consider feedback-assisted four-ports and resonant four-ports. Feedback-assisted four-ports are those where some, but not all, of the ports of the cascaded network are either terminated with partially reflecting mirrors, or connected to each other through a feedback circuit. A resonant circuit is obtained when all four ports of the cascaded network are terminated with reflectors or connected by feedback lines.

In Section II, a generalized lumped-element 2 × 2 coupler is described. This is an artificial device, which is instrumental in reducing a four-port circuit to a set of cascaded components. In Section III, the cascaded network, a four-port comprised of all the interconnected building blocks, is discussed. Section IV deals with the feedback-assisted configurations, while Section V addresses the seven possible resonator configurations. Section VI presents several examples illustrating how the generalized coupler can simplify circuit topology. Part II of this paper describes numerical experiments that demonstrate the utility of the present method.

II. The Generalized 2 × 2 Coupler

Two matrix representations will be used to describe circuit components. The first is a scattering transfer representation defined by the linear input/output relation

$$[a_1 \quad b_1 \quad a_2 \quad b_2]^T = \boldsymbol{A}[b_3 \quad a_3 \quad b_4 \quad a_4]^T \qquad (1)$$

where $\boldsymbol{A}$ is the scattering transfer matrix, a_i and b_i are, respectively, the incident and reflected waves at the ith port, as shown in Fig. 1, and the T superscript signifies transposition. The second representation defines the scattering matrix

$$[b_1 \quad b_2 \quad b_3 \quad b_4]^T = \boldsymbol{S}[a_1 \quad a_2 \quad a_3 \quad a_4]^T. \qquad (2)$$

Manuscript received September 2, 1997. This work was supported by the Natural Sciences and Engineering Research Council of Canada, and by the Fonds pour la Formation de Chercheurs et l'Aide à la Recherche.

The author is with the Department of Electrical and Computer Engineering, Concordia University, Montréal, P.Q., Canada H3G 1M8.

Publisher Item Identifier S 0018-9480(98)07248-2.

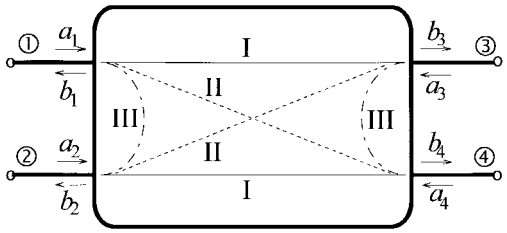

Fig. 1. Generalized lumped element 2 × 2 coupler. The paths denoted by I–III depict either a direct or a coupled connection between ports. (Table I describes the six possible coupler types.)

TABLE I
TYPES OF GENERALIZED LUMPED-ELEMENT 2 × 2 COUPLERS. (REFER TO FIG. 1)

Type	Direct Connection	Coupled Connection
1	I	II
2	II	I
3	I	III
4	III	I
5	III	II
6	II	III

The scattering transfer representation is used to evaluate the performance of a network of cascaded components, whereas the scattering matrix representation is convenient because most measuring instruments provide us with $\boldsymbol{S}$-parameter data, and group delay can be easily expressed in terms of its elements. The wave amplitudes a_i and b_i are linearly related to electric- and magnetic-field components (voltage and current). Of the several conventions in use [26], two are discussed in Section III.

On occasion, e.g., when the $\boldsymbol{A}$ matrix must be converted into an $\boldsymbol{S}$ matrix, it is convenient to use other scattering transfer matrices, such as a permuted version of $\boldsymbol{A}$, which we shall call the $\boldsymbol{T}$ matrix, or the inverse of $\boldsymbol{A}$, which we shall call $\boldsymbol{M}$. The results presented in this paper can also be formulated in terms of these alternative representations; however, we shall make little use of them.

There are six conceivable configurations for a lumped-element 2 × 2 coupler, each having two pairs of port connection, as shown in Fig. 1. The six possible configurations are listed in Table I. In the ordinary forward coupler, connections denoted as **I**'s represent direct connections between ports 1 and 3, and 2 and 4, respectively, **II**'s are coupled connections, and **III**'s do not exist. We shall call this a Type-1 coupler. The Type-2 coupler differs from the Type 1 in that, here, connections **II** are direct and connections I are coupled. Thus, Type 2 obtains from Type 1 by interchanging ports 3 and 4. The backward coupler, where **I**'s and **III**'s represent direct and coupled connections, respectively, is called Type 3, while the Type-4 coupler is a backward coupler rotated 90° in the plane of the paper around the center of the coupler. It can be obtained from a Type-3 coupler by exchanging ports 2 and 3. Type 5 is a forward coupler rotated by 90° around the center of the coupler, as illustrated in [21, Fig. 7]. Finally, Type 6 is a backward coupler with ports 3 and 4 interchanged. All six couplers are assumed to be symmetric, both bilaterally (vertical symmetry axis) as well as transversally (horizontal symmetry axis). These symmetry properties constrain the matrix representing the coupler [27].[1] For example, the $\boldsymbol{S}$ matrix of a bilaterally symmetric network must satisfy the condition

$$\boldsymbol{S} = \begin{bmatrix} 0 & 0 & 1 & 0 \\ 0 & 0 & 0 & 1 \\ 1 & 0 & 0 & 0 \\ 0 & 1 & 0 & 0 \end{bmatrix} \boldsymbol{S} \begin{bmatrix} 0 & 0 & 1 & 0 \\ 0 & 0 & 0 & 1 \\ 1 & 0 & 0 & 0 \\ 0 & 1 & 0 & 0 \end{bmatrix} \tag{3}$$

while the $\boldsymbol{S}$ matrix of a transversally symmetric four-port must satisfy the condition

$$\boldsymbol{S} = \begin{bmatrix} 0 & 1 & 0 & 0 \\ 1 & 0 & 0 & 0 \\ 0 & 0 & 0 & 1 \\ 0 & 0 & 1 & 0 \end{bmatrix} \boldsymbol{S} \begin{bmatrix} 0 & 1 & 0 & 0 \\ 1 & 0 & 0 & 0 \\ 0 & 0 & 0 & 1 \\ 0 & 0 & 1 & 0 \end{bmatrix}. \tag{4}$$

The corresponding conditions applicable in the $\boldsymbol{A}$ matrix representation are, respectively,

$$\boldsymbol{A}^{-1} = \begin{bmatrix} 0 & 1 & 0 & 0 \\ 1 & 0 & 0 & 0 \\ 0 & 0 & 0 & 1 \\ 0 & 0 & 1 & 0 \end{bmatrix} \boldsymbol{A} \begin{bmatrix} 0 & 1 & 0 & 0 \\ 1 & 0 & 0 & 0 \\ 0 & 0 & 0 & 1 \\ 0 & 0 & 1 & 0 \end{bmatrix} \tag{5}$$

and

$$\boldsymbol{A} = \begin{bmatrix} 0 & 0 & 1 & 0 \\ 0 & 0 & 0 & 1 \\ 1 & 0 & 0 & 0 \\ 0 & 1 & 0 & 0 \end{bmatrix} \boldsymbol{A} \begin{bmatrix} 0 & 0 & 1 & 0 \\ 0 & 0 & 0 & 1 \\ 1 & 0 & 0 & 0 \\ 0 & 1 & 0 & 0 \end{bmatrix}. \tag{6}$$

The $\boldsymbol{A}$ matrix representations of the six lumped-element couplers are given in Appendix A. They are all unimodular. The corresponding $\boldsymbol{S}$ matrix representations can be obtained from these, using the conversion formula

$$\boldsymbol{S} = \begin{bmatrix} \boldsymbol{T}_C \boldsymbol{T}_A^{-1} & \boldsymbol{T}_D - \boldsymbol{T}_C \boldsymbol{T}_A^{-1} \boldsymbol{T}_B \\ \boldsymbol{T}_A^{-1} & -\boldsymbol{T}_A^{-1} \boldsymbol{T}_B \end{bmatrix} \tag{7}$$

where

$$\boldsymbol{T} = \begin{bmatrix} \boldsymbol{T}_A & \boldsymbol{T}_B \\ \boldsymbol{T}_C & \boldsymbol{T}_D \end{bmatrix} = \Pi_{23} \boldsymbol{A} \Pi_{23}$$

and

$$\Pi_{23} = \begin{bmatrix} 1 & 0 & 0 & 0 \\ 0 & 0 & 1 & 0 \\ 0 & 1 & 0 & 0 \\ 0 & 0 & 0 & 1 \end{bmatrix}.$$

The $\boldsymbol{A}$ and $\boldsymbol{S}$ matrices of the generalized 2 × 2 couplers have eight nonzero elements arranged in a pattern characteristic of the coupler. Of the nonzero elements of the $\boldsymbol{A}$ matrices, only four are distinct, whereas in the corresponding $\boldsymbol{S}$ matrices, only two elements are distinct as a result of the symmetry constraint imposed by reciprocity. Denoting the power-coupling coefficient by K and the coupler-loss coefficient by a, one can show that for all six scattering matrices $\det[\boldsymbol{S}] = a^4$ and $\mathrm{eig}[\boldsymbol{S}] = \pm a[\sqrt{1-K} \pm j\sqrt{K}]$.

[1] Note: the typographic error in the last entry of (10), where the elements of the bottom row of σ_3 are interchanged, and the missing † superscript, indicating Hermitian conjugation, in all entries in column under "Losslessness" in Table I, e.g., $T^{-1} = \sigma_1 T \sigma_1$ should read $T^{-1} = \sigma_1 T^{\dagger} \sigma_1$.

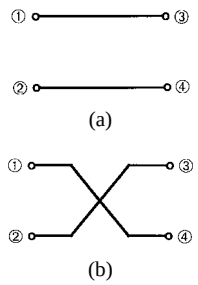

Fig. 2. Uncoupled pair of (a) parallel and (b) crossed transmission lines.

Although most interferometric circuits are fabricated with lumped element (fused) couplers, distributed parameter couplers can be included in the cascaded circuit. Of these, there are only two, namely, the forward and reverse coupler. For sake of completeness, their scattering transfer matrices are included in Appendix A.

III. The Cascaded Network

In addition to 2×2 couplers, the basic building blocks of the cascaded network include a pair of uncoupled waveguides that connect the couplers, a pair of partially reflecting mirrors and a pair of interfaces, encountered when, e.g., a pair of waveguides is spliced to one side of a 2×2 coupler. The scattering transfer matrix of a pair of uncoupled parallel waveguides, shown in Fig. 2(a), is

$$\boldsymbol{A} = \begin{bmatrix} e^{j\theta_1} & 0 & 0 & 0 \\ 0 & e^{-j\theta_1} & 0 & 0 \\ 0 & 0 & e^{j\theta_2} & 0 \\ 0 & 0 & 0 & e^{-j\theta_2} \end{bmatrix} \tag{8}$$

where $\theta_i = (\beta_i - j\alpha_i)l_i$, $i = 1, 2$ is the complex "electrical" length of line i, whose physical length is l_i, and the (possibly wavelength dependent) attenuation coefficient is α_i. Gain can be accommodated through a negative α_i. When the transmission lines are crossed, as in Fig. 2(b), a transformation, appropriate to exchanging ports 3 and 4 must be applied to (8).

A pair of lossless interfaces can be described by

$$\boldsymbol{A} = \begin{bmatrix} \dfrac{1}{\tau_1} & \dfrac{\rho_1}{\tau_1} & 0 & 0 \\ \dfrac{\rho_1}{\tau_1} & \dfrac{1}{\tau_1} & 0 & 0 \\ 0 & 0 & \dfrac{1}{\tau_2} & \dfrac{\rho_2}{\tau_2} \\ 0 & 0 & \dfrac{\rho_2}{\tau_2} & \dfrac{1}{\tau_2} \end{bmatrix} \tag{9}$$

where ρ_i and τ_i are, respectively, the reflection and transmission coefficients of the ith interface. For a lossless interface, these must satisfy the power conservation condition

$$\rho_i^2 + \tau_i^2 = 1, \qquad i = 1, 2. \tag{10}$$

For a pair of lossless mirrors, the scattering transfer matrix is

$$\boldsymbol{A} = j\begin{bmatrix} -\dfrac{1}{t_1} & \dfrac{r_1}{t_1} & 0 & 0 \\ -\dfrac{r_1}{t_1} & \dfrac{1}{t_1} & 0 & 0 \\ 0 & 0 & -\dfrac{1}{t_2} & \dfrac{r_2}{t_2} \\ 0 & 0 & -\dfrac{r_2}{t_2} & \dfrac{1}{t_2} \end{bmatrix} \tag{11}$$

where power conservation requires that

$$r_i^2 + t_i^2 = 1, \qquad i = 1, 2. \tag{12}$$

Splice loss in a cascaded network can most easily be taken into account by lumping it with the loss of the adjoining coupler. A brief discussion on the relationship between the mirror reflection and transmission coefficients r and t and their interface analogues ρ and τ is given in Appendix B.

Gratings play an important role in spectral filters and frequency selective interferometric networks. They are used as frequency selective mirrors terminating a transmission line, or embedded in waveguides connecting two couplers, or serving as a feedback circuit. Often, two gratings are configured back-to-back with a narrow gap between them and used as a Fabry–Perot resonator integrated into the interferometric device. A simple method to simulate the effect of such gratings is to set up their transfer matrix by concatenating the $\boldsymbol{A}$ matrices of interfaces and uniform waveguide sections in the order they appear in the grating. For example, the $\boldsymbol{A}$ matrix of a grating embedded in an optical fiber, as shown in Fig. 3, is

$$\boldsymbol{A} = \boldsymbol{A}_{fa}[\boldsymbol{A}_a\boldsymbol{A}_{ab}\boldsymbol{A}_b\boldsymbol{A}_{ba}]^2\boldsymbol{A}_a\boldsymbol{A}_{af} \tag{13}$$

where

$$\boldsymbol{A}_i = \begin{bmatrix} e^{j\phi_i} & 0 \\ 0 & e^{-j\phi_i} \end{bmatrix}, \qquad i = a, b$$

represents the uniform sections with ϕ_i being their complex phase delay, and

$$\boldsymbol{A}_{jk} = \frac{1}{2}\begin{bmatrix} \sqrt{\dfrac{n_j}{n_k}} + \sqrt{\dfrac{n_k}{n_j}} & \sqrt{\dfrac{n_j}{n_k}} - \sqrt{\dfrac{n_k}{n_j}} \\ \sqrt{\dfrac{n_j}{n_k}} - \sqrt{\dfrac{n_k}{n_j}} & \sqrt{\dfrac{n_j}{n_k}} + \sqrt{\dfrac{n_k}{n_j}} \end{bmatrix} \tag{14}$$

is the transfer matrix of the interface between dielectric media characterized by refractive indices n_j on the left and n_k on the right. In order to ensure that $\boldsymbol{A}_{jk}$ be unimodular, we define normalized incident and reflected waves through the linear transformation

$$\begin{bmatrix} a \\ b \end{bmatrix} = \frac{1}{\sqrt{2}}\begin{bmatrix} \sqrt{Y} & \sqrt{Z} \\ \sqrt{Y} & -\sqrt{Z} \end{bmatrix}\begin{bmatrix} \eta_0^{-(1/2)}E \\ \eta_0^{1/2}H \end{bmatrix} \tag{15}$$

rather than through the also familiar relation

$$\begin{bmatrix} a \\ b \end{bmatrix} = \frac{1}{\sqrt{2}}\begin{bmatrix} 1 & Z \\ 1 & -Z \end{bmatrix}\begin{bmatrix} \eta_0^{-(1/2)}E \\ \eta_0^{1/2}H \end{bmatrix} \tag{16}$$

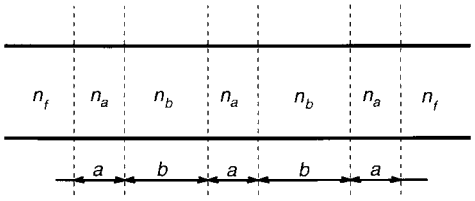

Fig. 3. A periodic grating embedded in an optical fiber n_f: refractive index of the fiber. n_a, n_b: refractive indices of the grating regions.

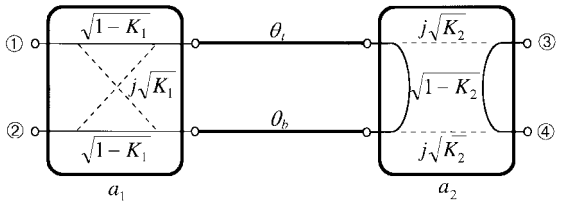

Fig. 4. Cascaded network example showing path transmissivities. The first coupler is Type 1, the second Type 4.

where $\eta_0 = \sqrt{\mu_0/\varepsilon_0}$ is the free-space impedance and E and H are the electric- and magnetic-field components in the plane of the interface.

By concatenating couplers, splices, mirrors, and transmission lines (waveguides), one can model a wide variety of microwave and optical circuits, as indicated in Section I and discussed in some detail in Section VI. The cascaded network so obtained is a four-port whose $\boldsymbol{A}$ matrix is the product of the scattering transfer matrices of the components in the order they are connected to each other in the circuit. Once again, (7) can be used to determine the $\boldsymbol{S}$ matrix of the cascaded network.

Interestingly, the scattering matrix of a cascaded network can be obtained by simple inspection. An example is given here by writing down the (1, 1), (1, 2), and (1, 3) elements of the $\boldsymbol{S}$ matrix of the network shown in Fig. 4, consisting of a Types-1 and -4 coupler. To obtain S_{11}, the transmission coefficients of all possible paths from port 1 back to port 1 must be added. Thus,

$$S_{11} = j2a_1^2 a_2 \sqrt{K_1(1-K_1)(1-K_2)}e^{-j(\theta_t+\theta_b)}. \tag{17}$$

Similarly, to obtain S_{12} or S_{13}, one must sum all possible paths from port 2 to port 1, or from port 3 to port 1, respectively. In the first case, there are two paths, therefore,

$$S_{12} = a_1^2 a_2 (1-2K_1)\sqrt{1-K_2}e^{-j(\theta_t+\theta_b)} \tag{18}$$

whereas, in the second case, there is only one, resulting in

$$S_{13} = ja_1 a_2 \sqrt{K_2(1-K_1)}e^{-j\theta_t}. \tag{19}$$

IV. Feedback-Assisted Four-Ports

Desirable performance for interferometers and filters are often obtained from feedback-assisted four-ports. The feedback can be internal, caused by a reflective element applied to one or several of the external ports of the cascaded circuit, or it can be external, caused by a waveguide or other transmission-circuit connecting external ports. In our case, the four-port is the cascaded network which is reduced by feedback elements to either a one- or two-port circuit. (The case when one port of the cascaded network is terminated, leaving a three port as the resultant network, will be disregarded. The case when two feedback-assisted three-ports are connected at their open ports can be treated, once again, as a cascaded network.) The so-called embedding network consists of circuit elements external to the cascaded network. The embedding network is characterized by its own scattering matrix $\boldsymbol{S}_E$ as follows:

$$\boldsymbol{a}_E = \boldsymbol{S}_E \boldsymbol{b}_E \tag{20}$$

where $\boldsymbol{a}_E$ and $\boldsymbol{b}_E$ are the column vectors of waves leaving and entering the embedding network, respectively.

Optical-fiber one-port circuits, essentially composite reflectors, have been investigated by Urquhart *et al.* [13], [28]. There are four possible feedback configurations, listed in Table II(a), which result in a one-port or (imperfect) mirror. The complex reflection coefficient of the mirror is obtained from the scattering matrix of the cascaded network $\boldsymbol{S}$, and from $\boldsymbol{S}_E$ according to

$$\Gamma = S_{11} + \boldsymbol{S}_{i1}(\boldsymbol{S}_E^{-1} - \boldsymbol{S}_{ii})^{-1}\boldsymbol{S}_{i1}, \qquad i = 2, 3, 4 \tag{21}$$

where $\boldsymbol{S}_{1i} = [S_{12}\ S_{13}\ S_{14}]$, $\boldsymbol{S}_{i1} = [S_{21}\ S_{31}\ S_{41}]^T$, and $\boldsymbol{S}_{ii}$ is a 3×3 submatrix of $\boldsymbol{S}$. For the four cases listed in Table II(a), the scattering matrix of the embedding network is, respectively,

1)
$$\boldsymbol{S}_E = \operatorname{diag}[r_2 \quad r_3 \quad r_4]$$

2)
$$\boldsymbol{S}_E = \begin{bmatrix} r_2 & 0 & t \\ 0 & r_3 & 0 \\ t & 0 & r_4 \end{bmatrix}$$

3)
$$\boldsymbol{S}_E = \begin{bmatrix} r_2 & t & 0 \\ t & r_3 & 0 \\ 0 & 0 & r_4 \end{bmatrix}$$

4)
$$\boldsymbol{S}_E = \begin{bmatrix} r_2 & 0 & 0 \\ 0 & r_3 & t \\ 0 & t & r_4 \end{bmatrix}$$

where r_i is the reflection coefficient of the mirror or feedback circuit at port i and t is the complex transmission coefficient of the feedback circuit. When the feedback circuit is a simple transmission line of length l, $t = \exp[-(\alpha+j\beta)l]$. Fixed attenuators, gratings, and Fabry–Perot resonators can be included in t as required, similarly r_i can represent the frequency-dependent reflection coefficient of gratings attached to the cascaded circuit. The magnitude of the mirror reflectivities must be between 0 and 1, the feedback path can have gain or loss.

Table II(b) lists the six possible configurations obtained when a cascaded four-port (with ports numbered, as in Fig. 1) is reduced to a two-port. In Cases 1–3, two reflective elements (mirrors) having complex reflection coefficients r_i terminate two of the four ports of the cascaded network. In Cases 4–6, a

TABLE II
FEEDBACK CONFIGURATIONS

Case	Ports terminated by mirrors	Ports connected by feedback line
1	2, 3 and 4	
2	3	2 to 4
3	4	2 to 3
4	2	3 to 4

(a)

Case	Ports terminated by mirrors	Ports connected by feedback line
1	2 and 4	
2	2 and 3	
3	3 and 4	
4		2 to 4
5		2 to 3
6		3 to 4

(b)

feedback circuit characterized by complex transmission and reflection coefficients t and r_i, respectively, connects two of the four ports. Both r_i and t are generally functions of frequency.

Through matrix manipulation, it can be shown that embedding results in a two-port scattering matrix given by

$$\boldsymbol{S}_r = \tilde{\boldsymbol{S}}_A + \tilde{\boldsymbol{S}}_B(\boldsymbol{S}_E^{-1} - \tilde{\boldsymbol{S}}_D)^{-1}\tilde{\boldsymbol{S}}_C \tag{22}$$

where $\tilde{\boldsymbol{S}} = \left[\begin{smallmatrix}\tilde{\boldsymbol{S}}_A & \tilde{\boldsymbol{S}}_B \\ \tilde{\boldsymbol{S}}_C & \tilde{\boldsymbol{S}}_D\end{smallmatrix}\right]$ is a transformed version of the 4×4 scattering matrix of the cascaded network $\boldsymbol{S}$, partitioned into 2×2 submatrices, obtained by exchanging columns and rows, i.e., applying permutation matrices to $\boldsymbol{S}$ until the dangling port parameters appear at the top of the $\boldsymbol{a}$ and $\boldsymbol{b}$ vectors. In particular, for Cases 1–6 of Table II(b), in consecutive order:

1)
$$\tilde{\boldsymbol{S}} = \Pi_{23}\boldsymbol{S}\Pi_{23} \quad \boldsymbol{S}_E = \mathrm{diag}[r_2 \;\; r_4]$$

2)
$$\tilde{\boldsymbol{S}} = \Pi_{24}\boldsymbol{S}\Pi_{24} \quad \boldsymbol{S}_E = \mathrm{diag}[r_3 \;\; r_2]$$

3)
$$\tilde{\boldsymbol{S}} = \boldsymbol{S} \quad \boldsymbol{S}_E = \mathrm{diag}[r_3 \;\; r_4]$$

4)
$$\tilde{\boldsymbol{S}} = \Pi_{23}\boldsymbol{S}\Pi_{23} \quad \boldsymbol{S}_E = \begin{bmatrix} r_2 & t \\ t & r_4 \end{bmatrix}$$

5)
$$\tilde{\boldsymbol{S}} = \Pi_{24}\boldsymbol{S}\Pi_{24} \quad \boldsymbol{S}_E = \begin{bmatrix} r_3 & t \\ t & r_2 \end{bmatrix}$$

6)
$$\tilde{\boldsymbol{S}} = \boldsymbol{S} \quad \boldsymbol{S}_E = \begin{bmatrix} r_3 & t \\ t & r_4 \end{bmatrix}$$

where Π_{ij} is the 4×4 permutation matrix obtained by interchanging the ith and jth rows and columns of the identity matrix.

Note that (22) is a special case of the $2N$-port cascaded network $N \geq 2$, embedded by a $2n$-port $n < N$, where $\tilde{\boldsymbol{S}}_A$, $\tilde{\boldsymbol{S}}_B$, $\tilde{\boldsymbol{S}}_C$, and $\tilde{\boldsymbol{S}}_D$ are $2(N-n) \times 2(N-n)$, $2(N-n) \times 2n$, $2n \times 2(N-n)$, and $2n \times 2n$ submatrices, respectively.

When feedback is the result of a circuit connecting two ports (Cases 4–6), the $\boldsymbol{A}_r$ matrix corresponding to $\boldsymbol{S}_r$ can be expressed through formulas similar to (22). For example, in Case 4,

$$\boldsymbol{A}_r = \boldsymbol{A}_A + \boldsymbol{A}_B(\boldsymbol{A}_E^{-1} - \boldsymbol{A}_D)^{-1}\boldsymbol{A}_C \tag{23}$$

whereas in Case 5,

$$\boldsymbol{A}_r = \boldsymbol{A}_B + \boldsymbol{A}_A(\boldsymbol{A}_E^{-1} - \boldsymbol{A}_C)^{-1}\boldsymbol{A}_D \tag{24}$$

where $\boldsymbol{A} = \left[\begin{smallmatrix}\boldsymbol{A}_A & \boldsymbol{A}_B \\ \boldsymbol{A}_C & \boldsymbol{A}_D\end{smallmatrix}\right]$ and, if the feedback line is matched, $\boldsymbol{A}_E = \left[\begin{smallmatrix} t^{-1} & 0 \\ 0 & t \end{smallmatrix}\right]$. These expressions have been presented elsewhere [29].

The so-called circulating waves inside the device are also of considerable interest. In Cases 1–3, these are the waves incident on, and reflected by, the external mirrors, whereas in Cases 4–6, they are the waves circulating in the feedback loop. The formalism presented above provides a simple expression to compute the complex wave amplitudes in the feedback path. Defining the 2×2 matrix,

$$\boldsymbol{U} = \boldsymbol{S}_E^{-1}(\boldsymbol{S}_E^{-1} - \tilde{\boldsymbol{S}}_D)^{-1}\tilde{\boldsymbol{S}}_C \tag{25}$$

where $\tilde{\boldsymbol{S}}$ and $\boldsymbol{S}_E$ have been given above, we obtain the complex circulating-wave amplitude, normalized to that of the incident amplitude, as one of the elements of $\boldsymbol{U}$ (assuming the other input is zero). Thus, e.g., in Case 1, where ports 2 and 4 are terminated by mirrors having reflection coefficients r_2 and r_4, respectively, the relative complex circulating amplitudes are

$$\frac{b_2}{a_1} = U_{11} \quad \frac{a_2}{a_1} = r_2 U_{11} \quad \frac{b_4}{a_1} = U_{21}$$

and

$$\frac{a_4}{a_1} = r_4 U_{21}. \tag{26}$$

Expressions for calculating the circulating-wave amplitudes in the remaining five cases, and conditions required to obtain a null in the reflected or transmitted intensities are given in Appendix C.

The formulas given in (25), (26), and Appendix C express the relative amplitudes of the circulating waves in the feedback path. When a circulating intensity is required at a location other than the feedback path, e.g., in the waveguides connecting the couplers, one must trace the wave through a coupler. As demonstrated at the end of Section III, and further examined in Part II of this paper, this is normally a straightforward task [30].

Of further interest is the group delay suffered by the reflected and transmitted signals. The group delay from ports j to i is defined by

$$\tau_{ij}(\omega) = -\mathrm{Im}\left(\frac{1}{S_{ij}}\frac{\partial S_{ij}}{\partial \omega}\right) \tag{27}$$

where S_{ij} is the appropriate element of $\boldsymbol{S}_r$. To facilitate comparing the performance of circuits operating at widely different wavelengths, we use the normalized group-delay parameter

$$\frac{c}{\lambda}\tau_{ij}(\omega) = \frac{\lambda}{2\pi}\,\mathrm{Im}\left(\frac{1}{S_{ij}}\frac{\partial S_{ij}}{\partial \lambda}\right) \tag{28}$$

TABLE III
RESONANT CIRCUITS

Option	Ports terminated by mirrors	Ports connected by feedback lines
1	1, 2, 3 and 4	
2	1 and 3	2 to 4
3	1 and 4	2 to 3
4	1 and 2	3 to 4
5		1 to 3, 2 to 4
6		1 to 4, 2 to 3
7		1 to 2, 3 to 4

where c and λ are the phase velocity and wavelength in vacuum or in the medium where the waves propagate.

It should be pointed out that the elements of the 2×2 scattering matrix of a feedback-assisted four-port can also be obtained by inspection, observing the properties of signal-flow graphs (Mason's rule), as demonstrated by Dowling and MacFarlane [31]. However, ours is a computational approach based on simple generic formulas; it is not our goal to present closed-form expressions applicable to a variety of circuit configurations.

V. RESONATOR CIRCUITS

The cascaded network discussed in Section III becomes a resonator when reflectors and/or feedback lines terminate all four ports. The seven possible configurations, here called "Options," are listed in Table III. The numbering of ports of the cascaded network is the same as that in Fig. 1. In Option 1, all four ports of the cascaded network are terminated by mirrors, in Options 2–4, two mirrors and a feedback circuit are used, while in Options 5–7, two separate feedback circuits are used.

The resonance condition for these seven distinct configurations can be formulated by a single expression as follows:

$$\det[\boldsymbol{I} - \boldsymbol{S}\boldsymbol{S}_E] = 0 \tag{29}$$

where $\boldsymbol{S}$ is the 4×4 scattering matrix of the cascaded network, and $\boldsymbol{S}_E$ is the scattering matrix of the embedding (terminating) network, which, in this case, is also a 4×4 matrix. In particular, for Options 1–7, in the following consecutive order:

Option 1)

$$\boldsymbol{S}_E = \operatorname{diag}[r_1 \;\; r_2 \;\; r_3 \;\; r_4]$$

Option 2)

$$\boldsymbol{S}_E = \begin{bmatrix} r_1 & 0 & 0 & 0 \\ 0 & r_2 & 0 & t \\ 0 & 0 & r_3 & 0 \\ 0 & t & 0 & r_4 \end{bmatrix}$$

Option 3)

$$\boldsymbol{S}_E = \begin{bmatrix} r_1 & 0 & 0 & 0 \\ 0 & r_2 & t & 0 \\ 0 & t & r_3 & 0 \\ 0 & 0 & 0 & r_4 \end{bmatrix}$$

Option 4)

$$\boldsymbol{S}_E = \begin{bmatrix} r_1 & 0 & 0 & 0 \\ 0 & r_2 & 0 & 0 \\ 0 & 0 & r_3 & t \\ 0 & 0 & t & r_4 \end{bmatrix}$$

Option 5)

$$\mathrm{S}_E = \begin{bmatrix} r_1 & 0 & t_1 & 0 \\ 0 & r_2 & 0 & t_2 \\ t_1 & 0 & r_3 & 0 \\ 0 & t_2 & 0 & r_4 \end{bmatrix}$$

Option 6)

$$\boldsymbol{S}_E = \begin{bmatrix} r_1 & 0 & 0 & t_1 \\ 0 & r_2 & t_2 & 0 \\ 0 & t_2 & r_3 & 0 \\ t_1 & 0 & 0 & r_4 \end{bmatrix}$$

Option 7)

$$\boldsymbol{S}_E = \begin{bmatrix} r_1 & t_1 & 0 & 0 \\ t_1 & r_2 & 0 & 0 \\ 0 & 0 & r_3 & t_2 \\ 0 & 0 & t_2 & r_4 \end{bmatrix}.$$

The determinant in (29) is complex valued. A null can only be obtained when both the phase and gain conditions of resonance are satisfied. In a passive circuit, this only occurs when there are no losses and the round-trip gain is unity. As losses rise, e.g., as a result of coupling to an external load, the absolute value of the determinant in (29) will no longer be zero at resonance, rather it will exhibit a minimum, at a point shifted slightly from the value of the independent variable marking the resonance of the lossless case. The rise and the corresponding shift of the minimum indicate that when losses are present, the gain condition cannot be satisfied and the phase condition is also affected. The minima reduce to nulls when sufficient gain is injected into the circuit to compensate for the losses incurred.

Numerous resonators are configured as cascaded circuits. An example is the multimirror Fabry–Perot resonator, an in-line device, which can incorporate a distributed parameter coupler in one of its cavities. When a cascaded network is configured as a resonator by attaching terminating networks to both sides, the condition of resonance can also be expressed in the form

$$\det[\boldsymbol{T}_C + \boldsymbol{T}_D\Gamma_R - \Gamma_L^{-1}\boldsymbol{T}_A - \Gamma_L^{-1}\boldsymbol{T}_B\Gamma_R] = 0 \tag{30}$$

where $\boldsymbol{T}_A$, $\boldsymbol{T}_B$, $\boldsymbol{T}_C$, and $\boldsymbol{T}_D$ are the 2×2 submatrices of the cascaded network $\boldsymbol{T}$ matrix, and Γ_L and Γ_R are the 2×2 reflection coefficient matrices of the left and right terminating circuits, respectively, i.e.,

$$\boldsymbol{S}_E = \begin{bmatrix} \Gamma_L & 0 \\ 0 & \Gamma_R \end{bmatrix}. \tag{31}$$

The feedback-assisted circuits of the previous section, or even the cascaded network itself, can be resonant if there is

at least one recirculating path in the device. A recirculating path can be a standing-wave resonator, such as a Fabry–Perot structure, or two mirrors attached to ports 2 and 4 of a forward coupler, or it can be a ring circuit where waves return to their point of origin by traveling in one direction only. Since resonances occur at every frequency where the round-trip phase is an integral multiple of 2π, the free spectral range (FSR) will be inversely proportional to the length of the recirculating path.

The finesse depends on the FSR and bandwidth of the resonance peak, i.e., on the losses in the path and those coupled into the path from the external portion of the circuit. In the class of interferometric circuits investigated here, there are often several resonant loops and, as a result, the FSR and finesse are not uniquely defined. For example, some configurations can have multiple resonances within the FSR, others can exhibit two interspersed sets of FSR's, etc. For this reason, we depend on a numerical evaluation of the finesse, extracted from a selected range of the computed frequency characteristics. Illustrative examples will be presented in Part II of this paper.

When a cascaded network has sufficient gain to overcome its losses, it will start to oscillate. Since there are usually several competitive threshold conditions, the oscillation frequency will be determined by the circuit parameters pertaining to the lowest threshold. At threshold, the existence of outgoing waves does not depend on the presence of incoming waves, therefore, (1) must have a solution for $a_i = 0$, $i = 1$–4. A nontrivial solution requires that

$$A_{11}A_{33} - A_{13}A_{31} = 0. \tag{32}$$

The four equations obtained from (1) with the incident amplitudes set to zero are solved for the relative amplitudes of the outgoing waves. Thus,

$$\begin{aligned} \frac{b_3}{b_1} &= -\frac{A_{13}}{\Delta} \\ \frac{b_4}{b_1} &= \frac{A_{11}}{\Delta} \\ \frac{b_2}{b_1} &= \frac{A_{11}A_{43} - A_{13}A_{41}}{\Delta} \end{aligned} \tag{33}$$

where $\Delta = A_{11}A_{23} - A_{13}A_{21}$.

VI. Circuit Equivalents

We shall illustrate the utility of the generalized coupler to convert intricate network topologies into a set of cascaded four-ports and also show the appropriate equivalent circuits, as categorized in Tables II and III.

Referring to the double- and triple-coupler (illustrated in Fig. 5) ring resonators or channel-dropping filters, first analyzed by Coale [1], and later by Oda [4] and Urquhart [28], we see that these configurations can be converted into a cascaded network with the use of the Type-5 coupler (see Fig. 6).

Both of the so-called bow-tie-shaped optical-fiber devices analyzed by Ja [32] reduce to the Case-6 feedback configuration, as shown in Fig. 7, where the cascaded network is made up of two couplers with transmission lines l_1 and l_2 separating

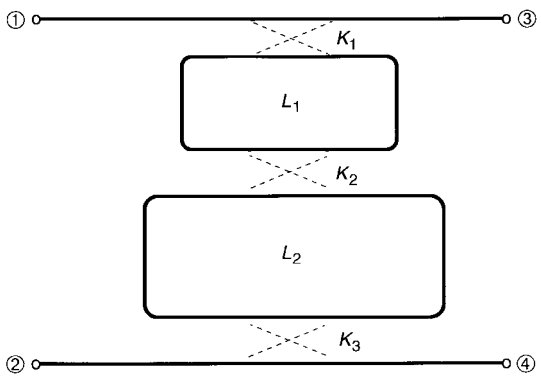

Fig. 5. Triple-coupler ring resonator. K_i are the power-coupling coefficients. L_i are the physical lengths of the resonant rings.

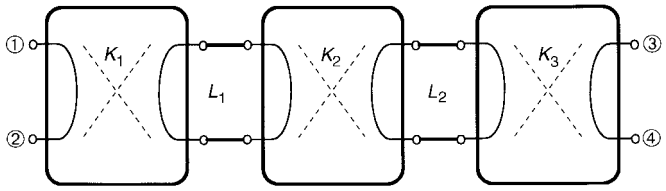

Fig. 6. Equivalent circuit of the triple-coupler ring resonator of Fig. 5, obtained using Type-5 couplers.

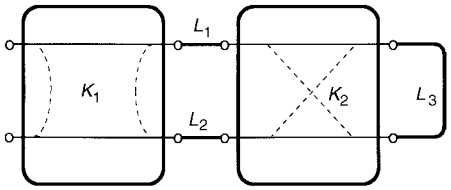

(a)

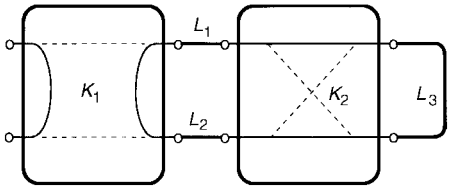

(b)

Fig. 7. Circuit equivalents of the so-called bow-tie-shaped fiber devices analyzed in [30]. (a) Fiber loop. (b) Fiber ring.

them. Fig. 7(a) is the equivalent circuit of the bow-tie-shaped optical-fiber loop, consisting of a Type-3 and -1 coupler, while Fig. 7(b) is the equivalent circuit of the bow-tie-shaped fiber ring, consisting of a Type-4 and -1 coupler.

The double-ring resonator described in [18] is also a Case-6 feedback configuration with two cascaded Type-3 (backward) couplers separated by two waveguides forming the cascaded network. On the other hand, both the symmetric [33] and nonsymmetric [34] S-shaped double-coupler fiber devices described by Ja are Case-5 feedback configurations. In the symmetric S-shaped double-coupler device, the couplers of the cascaded network are both Type 3, whereas in the nonsymmetric variety, a forward and backward coupler make up the cascaded network.

Resonators where all four ports of the cascaded network are terminated independently (Option 1) have been the subject of attention in the past [22], [35], however, the other six options

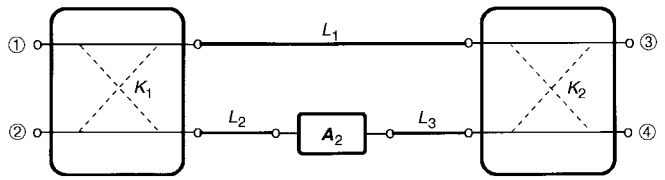

Fig. 8. Generic spectral filter configuration. $\boldsymbol{A}_2$ is the scattering transfer matrix of a feedback-assisted cascaded network.

have not been systematically treated. Note that Options 2 and 4 are equivalent only when the cascaded network consists of a single 2×2 coupler. The same comment applies to Options 5 and 7.

Since concatenation of two-ports is dealt with by simply multiplying their 2×2 scattering transfer matrices in the appropriate order, the present analysis can be applied to also treat systolic arrays [36] and spectral filters. An example of the first can be seen in [28, Fig. 8], where the unit cells of the chain are single Type-5 couplers embedded in Case-4 feedback. An altogether different device is obtained when the Type-5 coupler is replaced by a Type-4 coupler. A physical realization of the unit cell of this kind of systolic array consists of a forward coupler assisted by Case-5 feedback (or a reverse coupler with Case-6 feedback). Computed results on these arrays will be given in Part II of this paper.

Spectral filters are often configured as shown in Fig. 8, where a two-port, denoted by its scattering transfer matrix $\boldsymbol{A}_2$, itself a feedback-assisted cascaded network, is placed in one arm of a Mach–Zehnder interferometer. Spectral filters operating in the microwave and millimeter-wave region have first been treated in [2] and later for optical frequency division multiplexing (FDM) transmission systems by Oda *et al.* [37]. Numerical examples on these and other devices, including grating assisted interferometers, will be the subject of Part II of this paper.

VII. Conclusions

Through analysis and illustrative examples, we have demonstrated how readily a large class of interferometric circuits based on 2×2 couplers can be treated. By introducing a generalized lumped-element 2×2 coupler, we were able to reduce topological complexity to a set of cascaded four-ports, the so-called cascaded network, to which the frequently used transfer matrix analysis method was applied.

Simple analytic formulas were presented to calculate the transmission, reflection and time-delay characteristics of feedback-assisted four-ports and resonator circuits employing a cascaded network of possibly complex topology as a core. It was shown, by way of an example, how simple it is to obtain the $\boldsymbol{S}$ matrix of a cascaded four-port by inspection.

We enumerated four feedback-assisted one-port, six feedback-assisted two-ports, and seven resonator configurations that can be built with 2×2 couplers, reflectors, and transmission lines. Simple expressions were given to compute the circulating-wave amplitudes and the time-delay characteristics. Part II of this paper illustrates the economy and the wide-range capabilities of the present method.

A systematic approach to treat polarization sensitive (two-moded) interferometric circuits is the subject of work in progress. A similar investigation involving lumped-element 3×3 couplers has been concluded and will be submitted for publication in the near future.

Appendix A
Transfer Matrix Representation of Coupler Configurations

The scattering matrix of the lumped-element forward coupler (Type 1) is

$$\boldsymbol{S}_{[1]} = a \begin{bmatrix} 0 & 0 & \sqrt{1-K} & j\sqrt{K} \\ 0 & 0 & j\sqrt{K} & \sqrt{1-K} \\ \sqrt{1-K} & j\sqrt{K} & 0 & 0 \\ j\sqrt{K} & \sqrt{1-K} & 0 & 0 \end{bmatrix} \tag{A1}$$

where K is the power-coupling coefficient and $a = \sqrt{1-\gamma}$ is the loss coefficient (not to be confused with a_i, the incident wave at port i). The scattering matrices of the other five types are related to $\boldsymbol{S}_{[1]}$ via similarity transformations. These reflect the symmetry operations performed to transform one type into another, as described in Section II. Thus,

$$\begin{aligned} \boldsymbol{S}_{[2]} &= \Pi_{34}\boldsymbol{S}_{[1]}\Pi_{34} \\ \boldsymbol{S}_{[3]} &= \Pi_{24}\boldsymbol{S}_{[1]}\Pi_{24} \\ \boldsymbol{S}_{[4]} &= \Pi_{24}\Pi_{34}\boldsymbol{S}_{[1]}\Pi_{34}\Pi_{24} \\ \boldsymbol{S}_{[5]} &= \Pi_{23}\boldsymbol{S}_{[1]}\Pi_{23} \\ \boldsymbol{S}_{[6]} &= \Pi_{34}\Pi_{24}\boldsymbol{S}_{[1]}\Pi_{24}\Pi_{34} \end{aligned} \tag{A2}$$

where Π_{ij} is the 4×4 permutation matrix obtained by interchanging the ith and jth rows and columns of the identity matrix.

From these, the scattering transfer matrices of the six types of 2×2 couplers are computed as follows:

$$\boldsymbol{A}_{[1]} = \begin{bmatrix} \dfrac{\sqrt{1-K}}{a} & 0 & -j\dfrac{\sqrt{K}}{a} & 0 \\ 0 & a\sqrt{1-K} & 0 & ja\sqrt{K} \\ -j\dfrac{\sqrt{K}}{a} & 0 & \dfrac{\sqrt{1-K}}{a} & 0 \\ 0 & ja\sqrt{K} & 0 & a\sqrt{1-K} \end{bmatrix} \tag{A3}$$

$$\boldsymbol{A}_{[2]} = \begin{bmatrix} j\dfrac{\sqrt{K}}{a} & 0 & -\dfrac{\sqrt{1-K}}{a} & 0 \\ 0 & ja\sqrt{K} & 0 & a\sqrt{1-K} \\ -\dfrac{\sqrt{1-K}}{a} & 0 & j\dfrac{\sqrt{K}}{a} & 0 \\ 0 & a\sqrt{1-K} & 0 & ja\sqrt{K} \end{bmatrix} \tag{A4}$$

$$\boldsymbol{A}_{[3]} = \frac{1}{\sqrt{1-K}} \begin{bmatrix} \dfrac{1}{a} & 0 & 0 & -j\sqrt{K} \\ 0 & a & j\sqrt{K} & 0 \\ 0 & -j\sqrt{K} & \dfrac{1}{a} & 0 \\ j\sqrt{K} & 0 & 0 & a \end{bmatrix} \tag{A5}$$

$$\boldsymbol{A}_{[4]}=\frac{j}{\sqrt{K}}\begin{bmatrix}-\frac{1}{a} & 0 & 0 & \sqrt{1-K}\\ 0 & a & -\sqrt{1-K} & 0\\ 0 & \sqrt{1-K} & -\frac{1}{a} & 0\\ -\sqrt{1-K} & 0 & 0 & a\end{bmatrix} \tag{A6}$$

$$\boldsymbol{A}_{[5]}=\frac{j}{\sqrt{K}}\begin{bmatrix}0 & \sqrt{1-K} & -\frac{1}{a} & 0\\ -\sqrt{1-K} & 0 & 0 & a\\ -\frac{1}{a} & 0 & 0 & \sqrt{1-K}\\ 0 & a & -\sqrt{1-K} & 0\end{bmatrix} \tag{A7}$$

$$\boldsymbol{A}_{[6]}=\frac{1}{\sqrt{1-K}}\begin{bmatrix}0 & -j\sqrt{K} & \frac{1}{a} & 0\\ j\sqrt{K} & 0 & 0 & a\\ \frac{1}{a} & 0 & 0 & -j\sqrt{K}\\ 0 & a & j\sqrt{K} & 0\end{bmatrix}. \tag{A8}$$

In addition to the lumped-element couplers, we also list the transfer matrices of the distributed parameter forward and backward couplers. For the forward coupler,

$$\boldsymbol{A}=\begin{bmatrix}pe^{j\beta_0 x} & 0 & q^*e^{j\beta_0 x} & 0\\ 0 & p^*e^{-j\beta_0 x} & 0 & qe^{-j\beta_0 x}\\ q^*e^{j\beta_0 x} & 0 & p^*e^{j\beta_0 x} & 0\\ 0 & qe^{-j\beta_0 x} & 0 & pe^{-j\beta_0 x}\end{bmatrix} \tag{A9}$$

where $p=\cos(\zeta x)+j(\Delta\beta/2\zeta)\sin(\zeta x)$, $q=j(\kappa/\zeta)\sin(\zeta x)$, x is the direction of propagation, $\zeta=\sqrt{(\Delta\beta/2)^2+\kappa^2}$, $\Delta\beta=\beta_1-\beta_2$, $\beta_0=\frac{1}{2}(\beta_1+\beta_2)$, β_i are the real propagation constants of the coupled guides, κ is the real coupling coefficient, and the star refers to conjugation. The transfer matrix of the distributed backward coupler is shown in (A10), at the bottom of this page, where now $p=\cos(\zeta x)+j(\beta_0/\zeta)\sin(\zeta x)$, $q=-j(\kappa/\zeta)\sin(\zeta x)$, and $\zeta=\sqrt{\beta_0^2-\kappa^2}$.

Appendix B
Matrix Representations for an Interface and a Mirror

The scattering matrix and corresponding transfer matrix of a single lossless interface are, respectively,

$$\boldsymbol{S}=\begin{bmatrix}\rho & \tau\\ \tau & -\rho\end{bmatrix}\quad\text{and}\quad\boldsymbol{A}=\frac{1}{\tau}\begin{bmatrix}1 & \rho\\ \rho & 1\end{bmatrix} \tag{A11}$$

where ρ is the amplitude reflection coefficient and $\tau=\sqrt{1-\rho^2}$ is the amplitude transmission coefficient. A thin mirror is formed by two interfaces separated by a distance, i.e., a length of transmission line. By arbitrarily selecting the phase shift through this transmission line to be $\varphi=-\pi/2$ and the mirror to be bilaterally symmetric, we obtain the scattering transfer matrix of the mirror

$$\boldsymbol{A}_M=\frac{j}{t}\begin{bmatrix}-1 & r\\ -r & 1\end{bmatrix} \tag{A12}$$

where $r=2\rho/(1+\rho^2)$ and $t=(1-\rho^2)/(1+\rho^2)$. The corresponding scattering matrix is

$$\boldsymbol{S}_M=\begin{bmatrix}r & jt\\ jt & r\end{bmatrix}. \tag{A13}$$

Appendix C
Circulating-Wave Amplitudes for Feedback-Assisted Four-Ports

In this Appendix, expressions are given for the relative amplitudes of the circulating waves, and for the conditions to obtain a null in the output power at one of the open ports in feedback-assisted cascaded circuits.

With the $\boldsymbol{U}$ matrix defined as in (25), and with wave amplitude designations shown in Fig. 1, the circulating-wave amplitudes of Cases 2–6 are listed below. It is assumed that only port 1 is excited:

Case 2)

$$\begin{aligned}\frac{b_2}{a_1}&=U_{21}\quad\frac{a_2}{a_1}=r_2U_{21}\\ \frac{b_3}{a_1}&=U_{11}\quad\frac{a_3}{a_1}=r_3U_{11}\end{aligned} \tag{A14}$$

Case 3)

$$\begin{aligned}\frac{b_3}{a_1}&=U_{11}\quad\frac{a_3}{a_1}=r_3U_{11}\\ \frac{b_4}{a_1}&=U_{21}\quad\frac{a_4}{a_1}=r_4U_{21}\end{aligned} \tag{A15}$$

Case 4)

$$\begin{aligned}\frac{b_2}{a_1}&=U_{11}\quad\frac{a_2}{a_1}=r_2U_{11}+tU_{21}\\ \frac{b_4}{a_1}&=U_{21}\quad\frac{a_4}{a_1}=tU_{11}+r_4U_{21}\end{aligned} \tag{A16}$$

Case 5)

$$\begin{aligned}\frac{b_2}{a_1}&=U_{21}\quad\frac{a_2}{a_1}=tU_{11}+r_2U_{21}\\ \frac{b_3}{a_1}&=U_{11}\quad\frac{a_3}{a_1}=r_3U_{11}+tU_{21}\end{aligned} \tag{A17}$$

$$\boldsymbol{A}=\begin{bmatrix}pe^{j(\Delta\beta/2)x} & 0 & 0 & q^*e^{j(\Delta\beta/2)x}\\ 0 & p^*e^{-j(\Delta\beta/2)x} & qe^{-j(\Delta\beta/2)x} & 0\\ 0 & q^*e^{-j(\Delta\beta/2)x} & pe^{-j(\Delta\beta/2)x} & 0\\ qe^{j(\Delta\beta/2)x} & 0 & 0 & p^*e^{j(\Delta\beta/2)x}\end{bmatrix} \tag{A10}$$

Case 6)

$$\frac{b_3}{a_1} = U_{11} \quad \frac{a_3}{a_1} = r_3 U_{11} + t U_{21}$$
$$\frac{b_4}{a_1} = U_{21} \quad \frac{a_4}{a_1} = t U_{11} + r_4 U_{21}. \qquad \text{(A18)}$$

When the circuit configuration gives rise to a reflected signal at the input port, a null in this reflected signal is obtained when $|(\boldsymbol{S}_r)_{11}| = 0$. This obviously does not apply to the so-called unit transmittance circuits [6], such as a cascaded circuit built with, e.g., two forward couplers, since in these configurations there is no reflected signal under ideal conditions. In contrast, a null in the output intensity requires that $|(\boldsymbol{S}_r)_{21}| = 0$. For feedback-assisted four-ports, $\boldsymbol{S}_r$ is given in (22).

REFERENCES

[1] F. S. Coale, "A traveling-wave directional filter," *IRE Trans. Microwave Theory Tech.*, vol. MTT-4, pp. 256–260, Oct. 1956.

[2] H. Kumazawa, I. Ohtomo, and S. Shimada, "A 30-GHz band periodic filter with a ring resonator," *Electron. Commun. Japan*, vol. 59-B, pp. 78–86, 1976.

[3] H. F. Schlaak, "Periodic spectral filter with integrated optical directional coupler," *Opt. Quantum Electron.*, vol. 13, pp. 181–186, 1981.

[4] K. Oda, N. Takato, and H. Toba, "A wide-FSR waveguide double-ring resonator for optical FDM transmission systems," *J. Lightwave Technol.*, vol. 9, pp. 728–736, June 1991.

[5] A. D. Drake and D. C. Leiner, "Fiber-optic interferometer for remote subångstrøm vibration measurement," *Rev. Sci. Instrum.*, vol. 55, pp. 162–165, 1984.

[6] H. van de Stadt, "Ring interferometers with unit transmittance," *Appl. Opt.*, vol. 24, pp. 2290–2292, 1985.

[7] D. A. Jackson, "Monomode optical fiber interferometers for precision measurement," *J. Phys. E, Sci. Instrum.*, vol. 18, pp. 981–1001, 1985.

[8] J. Stone and D. Marcuse, "Ultrahigh finesse fiber Fabry–Perot interferometers," *J. Lightwave Technol.*, vol. LT-4, pp. 382–385, Apr. 1986.

[9] R. W. C. Vance and R. Barrow, "General linear differential interferometers," *J. Opt. Soc. Amer. A, Opt. Image Sci.*. vol. 12, pp. 346–353, 1995.

[10] L. F. Stokes, M. Chodorow, and H. J. Shaw, "Sensitive all-single-mode-fiber resonant ring interferometer," *J. Lightwave Technol.*, vol. LT-1, pp. 110–115, Jan. 1983.

[11] R. R. A. Syms, "Resonant cavity sensor for integrated optics," *IEEE J. Quantum Electron.*, vol. QE-21, pp. 322–328, Apr. 1985.

[12] G. Böck, "Fiber-optic ring resonator with highly wavelength- selective input reflection coefficient," *Siemens Forsch.- & Entwickl.ber.*, vol. 15, pp. 150–156, 1986.

[13] P. Barnsley, P. Urquhart, C. Millar, and M. Brierley, "Fiber Fox–Smith resonators: Application to single-longitudinal-mode operation of fiber lasers," *J. Opt. Soc. Amer. A, Opt. Image Sci.*, vol. 5, pp. 1339–1346, 1988.

[14] F. Zhang and J. W. Y. Lit, "Direct coupling single-mode fiber ring resonator," *J. Opt. Soc. Amer. A, Opt. Image Sci.*, vol. 5, pp. 1347–1355, 1988.

[15] K. P. Jackson *et al.*, "Optical fiber delay-line signal processing," *IEEE Trans. Microwave Theory Tech.*, vol. MTT-33, pp. 193–210, Mar. 1985.

[16] C.-L. Chen, "Optical fiber Fabry–Perot cavities and recirculating delay lines as tunable microwave filters," *IEEE Trans. Microwave Theory Tech.*, vol. 38, pp. 647–653, May 1990.

[17] Y. H. Ja, "Simultaneous resonance of an s-shaped two-coupler optical fiber ring resonator," *Opt. Commun.*, vol. 102, pp. 133–140, 1993.

[18] J. C. Martin and M. P. Bernal, "Double ring and Fabry–Perot ring resonators: Application for an optical fiber laser," *Appl. Opt.*, vol. 33, pp. 4801–4806, 1994.

[19] G. Barbarossa, A. M. Matteo, and M. N. Armenise, "Theoretical analysis of triple-coupler ring-based optical guided-wave resonator," *J. Lightwave Technol.*, vol. 13, pp. 148–157, Feb. 1995.

[20] Y. H. Ja, "Generalized theory of optical fiber loop and ring resonators with multiple couplers, Part 2: General characteristics," *Appl. Opt.*, vol. 29, pp. 3524–3529, 1990.

[21] J. Capmany and M. A. Muriel, "A new transfer matrix formalism for the analysis of fiber ring resonators: Compound coupled structures for FDMA demultiplexing," *J. Lightwave Technol.*, vol. 8, pp. 1904–1919, Dec. 1990.

[22] F. Sanchez, "Matrix algebra for all-fiber optical resonators," *J. Lightwave Technol.*, vol. 9, pp. 838–844, July 1991.

[23] F. Zhang and J. W. Y. Lit, "Compound fiber ring resonator: Theory," *J. Opt. Soc. Amer. A, Opt. Image Sci.*, vol. 11, pp. 1867–1873, 1994.

[24] A. H. Quoc and S. Tedjini, "Experimental investigation on the optical unbalanced Mach–Zehnder interferometers as microwave filters," *IEEE Microwave Guided Wave Lett.*, vol. 4, pp. 183–185, June 1994.

[25] Y. H. Ja, X. Dai, and L. N. Binh, "Experimental study of a bow-tie-shaped optical fiber ring resonator with two 2×2 fiber couplers," *Appl. Opt.*, vol. 33, pp. 5594–5601, 1994.

[26] K. Kurokawa, *An Introduction to the Theory of Microwave Circuits.* New York: Academic, 1969, ch. 1.

[27] O. Schwelb and R. Antepyan, "Conservation laws for distributed four-ports," *IEEE Trans. Microwave Theory Tech.*, vol. MTT-33, pp. 157–160, Feb. 1985.

[28] P. Urquhart, "Compound optical-fiber based resonators," *J. Opt. Soc. Amer. A, Opt. Image Sci.*, vol. 5, pp. 803–812, 1988.

[29] E. Milczarek and O. Schwelb, "Feedback assisted optical couplers," in *Proc. Canadian Conf. Elect. Computer Eng.*, Vancouver, B.C., Canada, Sept. 14–17, 1993, pp. 1266–1269.

[30] L. N. Binh, N. Q. Ngo, and S. F. Luk, "Graphical representation and analysis of the z-shaped double-coupler optical resonator," *J. Lightwave Technol.*, vol. 11, pp. 1782–1792, Nov. 1993.

[31] E. M. Dowling and D. L. MacFarlane, "Lightwave lattice filters for optically multiplexed communication systems," *J. Lightwave Technol.*, vol. 12, pp. 471–486, Mar. 1994.

[32] Y. H. Ja, "A bow-tie shaped optical fiber loop and ring with double couplers," *Fiber Integr. Opt.*, vol. 9, pp. 199–217, 1990.

[33] ———, "A symmetric s-shaped double-coupler optical-fiber loop," *J. Modern Opt.*, vol. 37, pp. 1297–1317, 1990.

[34] ———, "An unsymmetric s-shaped double-coupler optical fiber loop," *Opt. Commun.*, vol. 78, pp. 81–89, 1990.

[35] C.-L. Chen, "Directional coupler resonators as guided-wave optical components: A proposal," *Appl. Opt.*, vol. 26, pp. 2612–2617, 1987.

[36] B. Moslehi, M. Tur, J. W. Goodman, and H. J. Shaw, "Fiber optic lattice signal processing," *Proc. IEEE*, vol. 72, pp. 909–930, July 1984.

[37] K. Oda, N. Takato, H. Toba, and K. Nosu, "A wide-band guided-wave periodic multi/demultiplexer with a ring resonator for optical FDM transmission systems," *J. Lightwave Technol.*, vol. 6, pp. 1016–1023, June 1988.

Otto Schwelb (A'59–M'62–SM'85–LS'96) was born in Budapest, Hungary, in 1931. He received the Diploma in telecommunication engineering from the Technical University of Budapest, Budapest, Hungary, in 1954, and the Ph.D. degree in electrical engineering from McGill University, Montréal, P.Q., Canada, in 1978.

From 1957 to 1967, he was with the Research and Development Division, Northern Electric Company, where he worked on microwave communication systems. From 1967 to 1997, he was on the faculty of the Department of Electrical and Computer Engineering, Concordia University, Montréal, until his retirement in 1997. He continues to maintain an affiliation with Concordia University, as an Adjunct Professor. His research interests include guided electromagnetic-wave propagation in anisotropic media, surface acoustic-wave grating filters, and the design and modeling of interferometric sensor circuits.